

QSAR-Guided Generative Framework for the Discovery of Synthetically Viable Odorants

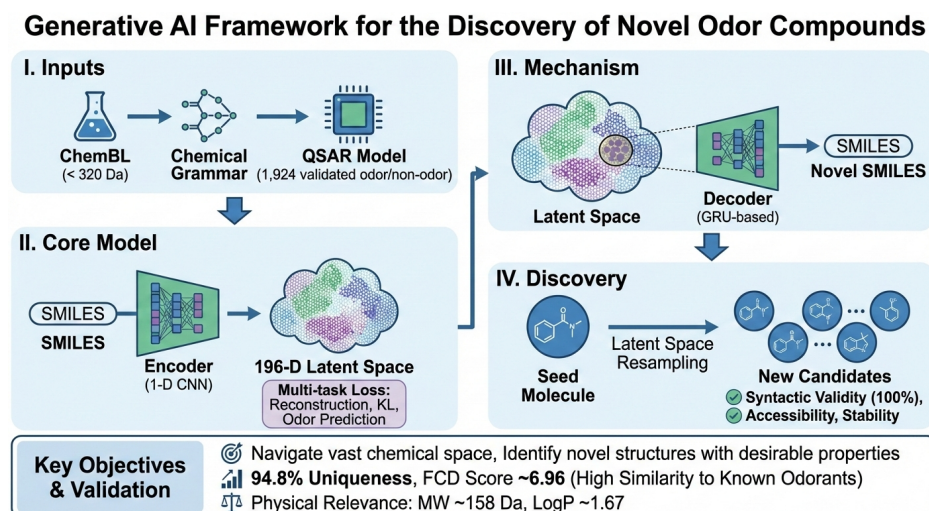
Tim C. Pearce^{*1} and Ahmed Ibrahim²

¹Biomedical Engineering Research Group, School of Engineering, University of Leicester, University Road, Leicester LE1 7RH, United Kingdom

²School of Clinical Medicine, University of Cambridge, Addenbrooke's Hospital, Hills Road, Cambridge CB2 0SP, United Kingdom

ABSTRACT

The discovery of novel odorant molecules is key for the fragrance and flavor industries, yet efficiently navigating the vast chemical space to identify structures with desirable olfactory properties remains a significant challenge. Generative artificial intelligence offers a promising approach for *de novo* molecular design but typically requires large sets of molecules to learn from. To address this problem, we present a framework combining a variational autoencoder (VAE) with a quantitative structure-activity relationship (QSAR) model to generate novel odorants from limited training sets of odor molecules. The self-supervised learning capabilities of the VAE allow it to learn SMILES grammar from ChEMBL database, while its training objective is augmented with a loss term derived from an external QSAR model to structure the latent representation according to odor probability. While the VAE demonstrated high internal consistency in learning the QSAR supervision signal, validation against an external, unseen ground truth dataset (Unique Good Scents) confirms the model generates syntactically valid structures (100% validity achieved via rejection sampling) and 94.8% unique structures. The latent space is effectively structured by odor likelihood, evidenced by a Fréchet ChemNet Distance (FCD) of ≈ 6.96 between generated molecules and known odorants, compared to ≈ 21.6 for the ChEMBL baseline. Structural analysis via Bemis-Murcko scaffolds reveals that 74.4% of candidates possess novel core frameworks distinct from the training data, indicating the model performs extensive chemical space exploration beyond simple derivatization of known odorants. Generated candidates display physicochemical properties consistent with ground-truth odorants (mean MW ~ 158 Da, LogP ~ 1.67) and comparable predicted ADMET profiles. Furthermore, quantum mechanical calculations (GFN2-xTB) verify thermodynamic stability with energy distributions matching known volatiles, and automated retrosynthesis demonstrates practical viability, yielding valid synthesis routes for 100% of candidates, averaging 2.89 steps from commercially available precursors. This integrated approach provides a novel and systematic methodology for applying generative AI to explore chemical space specifically for the discovery of new candidate odorant molecules.



Keywords: odorant molecules, olfaction, computational chemistry, molecule design, generative AI

*Corresponding author: t.c.pearce@le.ac.uk

Introduction

Olfactory perception (whether orthonasal or retronasal) fundamentally shapes consumer experience, making the discovery of new scents and flavors a key competitive advantage and an area of significant research investment [1]. This is a dynamic interdisciplinary endeavor, driven by the innovation needs of the fragrance and food industries, commercial demands for unique and cost-effective ingredients, increasingly stringent regulatory constraints regarding safety and environmental impact, and a growing imperative for sustainable and ethically sourced materials [2]. These factors necessitate a constant search not only for replacements for restricted ingredients but also for molecules offering enhanced performance, such as improved stability in challenging product matrices, novel olfactory characteristics that create new trends, and added consumer benefits like improved diffusion, longevity, or malodor counteraction [3]. Consequently, there is substantial interest in understanding structure-odor relationships (SORs) and developing new approaches for odor molecule discovery and design [4].

Understanding the link between molecular structure and perceived odor presents a formidable scientific challenge. Molecules must possess specific physicochemical properties: sufficient volatility, moderate hydrophobicity, and typically a molecular weight below ~300 Da to reach and interact with olfactory receptors (ORs) in the nasal epithelium [5]. The human olfactory system employs ~400 functional ORs in a complex combinatorial coding strategy, where single receptors recognize multiple odorants and single odorants activate multiple receptors [6]. This system produces a vast range of distinct perceived odors – while the exact number is debated, the potential perceptual odor space is immense, generated from a chemical space potentially spanning billions of discrete molecules [7]. The highly dimensional molecular and perceptual space is sensitive to subtle structural nuances; therefore, discovering new molecules with diverse structures is essential for industrial applications while also advancing our fundamental understanding of the olfactory pathway and odor perception.

Traditionally, novel odorant discovery relies heavily on synthetic organic chemistry, often guided by intuition and empirical observation based on known natural or synthetic odorants [1]. Chemists systematically modify structures or explore derivatives of readily available chemical feedstocks, iteratively synthesizing analogs and evaluating their scent organoleptically. While successful, this ‘molecule-first’ approach can be laborious and may struggle to efficiently navigate the vast potential chemical space to find truly novel structures meeting specific performance, property or safety criteria.

Recent advances in computational methods, particularly generative artificial intelligence (AI), offer powerful new tools to address these challenges. Over the past five years, techniques like variational autoencoders (VAEs), generative adversarial networks (GANs), transformers, and diffusion models have profoundly impacted molecular discovery, enabling rapid exploration of chemical space and *de novo* design [8–10]. These methods facilitate ‘inverse design’, shifting focus from modifying known structures to generating entirely new molecules optimized *a priori* to satisfy key property profiles [11]. By using desired characteristics as inputs, AI models propose candidates meeting complex multi-objective criteria. However, while this property-driven approach has shown success in yielding experimentally validated molecules for pharmaceutical targets [12], its application to the specific domain of olfaction remains comparatively limited. The discovery of novel odorants imposes uniquely stringent requirements—necessitating precise physicochemical properties for volatility alongside rigorous dermatological and environmental safety compliance—that generic molecular generators often fail to capture. Consequently, the field holds significant promise for accelerating odorant innovation only when these generative capabilities are tightly integrated with strict property checks and predictions of synthetic feasibility to bridge the gap between theoretical design and practical synthesis [13].

Generative AI approaches generally rely on large labeled datasets, which are often unavailable for specific properties like odor [14]. Directly training generative models on the limited sets of known odorants is insufficient to capture the complex syntax of SMILES or establish a continuous, interpolatable latent space. This paper introduces a framework to overcome this limitation. We combine a predictive quantitative structure-activity relationship (QSAR) model, trained on a curated set of known odorants, with a molecular variational autoencoder (VAE). This combined generative framework synergizes the representational power of a VAE with the predictive capability of a QSAR model tailored for odorant properties. The approach leverages the VAE’s ability to learn the underlying ‘grammar’ of molecular structures from large, general chemical databases (ChemBL) via self-supervision, while using the QSAR model’s predictions to specifically guide the VAE’s learning process and structure its latent space towards olfactory relevance.

The subsequent sections detail this integrated methodology: Section 2 outlines the VAE and QSAR model architectures and the combined training strategy; Section 3 presents the validation of the QSAR model and the VAE’s generative performance, with a primary focus on validating the physicochemical, structural, and electronic properties of the generated compounds against the generic chemical baseline (ChemBL) rather than benchmarking generative architectures; and Section 4 discusses the implications of this guided generative approach for accelerating the discovery of next-generation fragrance and flavor ingredients.

Methods

Molecular variational autoencoder architecture

The variational autoencoder architecture consists of four main components: an encoder, a latent space, an odor prediction head and a decoder. We base the VAE architecture on that reported in [15], adding a QSAR-driven odor prediction head (Figure 1).

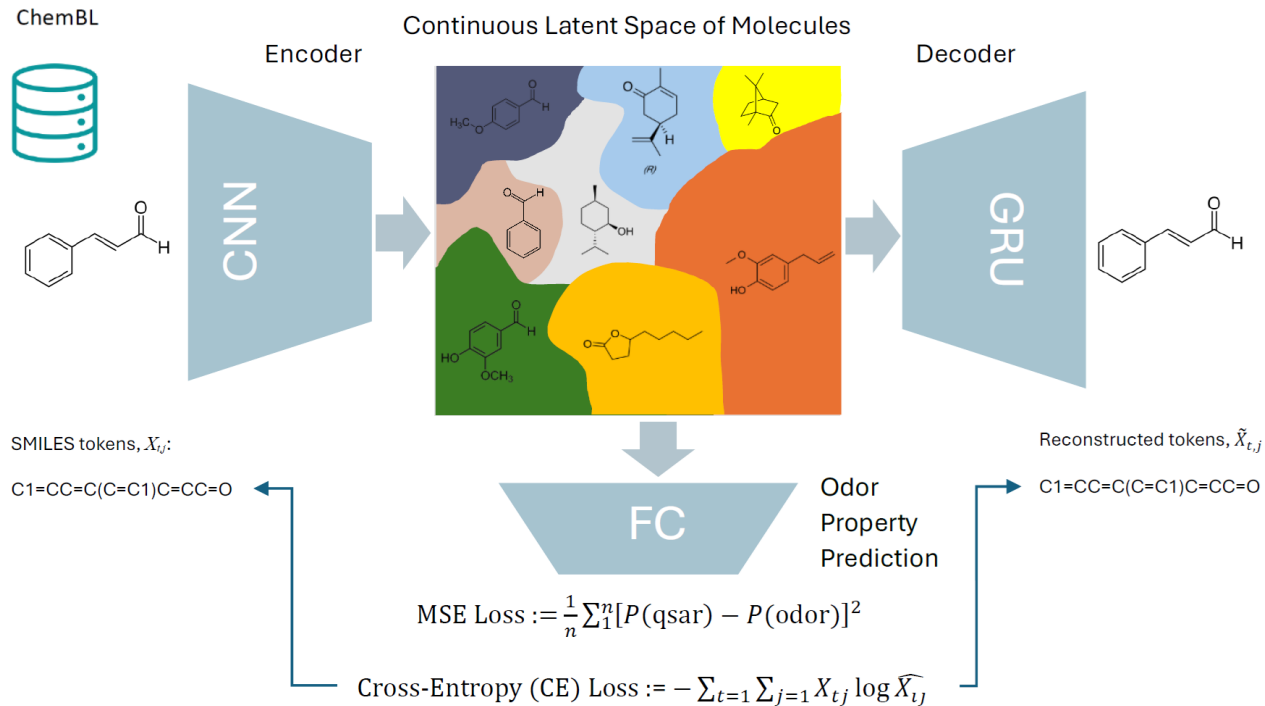


Figure 1. Variational Autoencoder framework concept. Abbreviations: CNN, convolutional neural network; GRU, gated recurrent unit; FC, fully connected (dense); KL, Kullback-Leibler divergence; Recon Loss, reconstruction loss (categorical cross-entropy); Prop Loss, property prediction loss (mean squared error, as described in text). The diagram illustrates the flow: input SMILES from ChemBL are processed by an Encoder (CNN based) mapping to a continuous latent space. Latent vectors z are input to both a Decoder (GRU based) for reconstructing SMILES sequences and an Odor Property Prediction head (FC based) predicting odor probability $P(\text{odor})$. The combined training objective minimizes the Recon Loss, the Prop Loss, and the KL divergence regularization term.

SMILES sequence embedding: A single input SMILES (Simplified Molecular Input Line Entry System) sequence is padded to a fixed length T , resulting in a character sequence $s' = (c_1, c_2, \dots, c_T)$, where each character c_t belongs to the predefined vocabulary \mathcal{C} of size V . This fixed length T is determined by the maximum sequence length observed across the entire training dataset to ensure no input molecule's representation is truncated. To represent this sequence numerically, one-hot encoding is performed. First, we define a mapping index $\mathcal{C} \rightarrow \{0, 1, \dots, V - 1\}$ that assigns a unique integer index to each character in the vocabulary. Each character c_t in s' is then transformed into a one-hot vector $v_t \in \{0, 1\}^V$, such that the j -th component of this vector (where j ranges from 0 to $V - 1$) is determined by comparing j with the unique index assigned to the character c_t , using the Kronecker delta

$$(v_t)_j = \delta_{j, \text{index}(c_t)}, \quad (1)$$

where $\delta_{a,b}$ equals 1 if $a = b$ and 0 otherwise.

These one-hot vectors are arranged into a matrix X of shape $T \times V$, where each row corresponds to a character token in the sequence. The scalar element $X_{t,j}$ at row t and column j of this matrix X is therefore given by

$$X_{t,j} = \delta_{j, \text{index}(c_t)} \quad \text{for } t \in \{1, \dots, T\}, j \in \{0, \dots, V - 1\}. \quad (2)$$

This means that for each row t of the matrix X , only the single element in the column j corresponding to the index of character c_t will be 1, and all other elements in that row will be 0. This matrix $X \in \{0, 1\}^{T \times V}$ serves as the input tensor to the VAE encoder.

VAE encoder: The encoder network maps an input SMILES token sequence to the parameters of a latent Gaussian distribution. Each SMILES (represented by input tensor X) is directly processed by the first 1-D convolution layer. In this context, the sequence length T serves as the steps (or length) dimension along which the 1-D convolution kernel slides. The vocabulary size V acts as the channels dimension; at each time step t , the channels map onto the elements of the V -dimensional one-hot vector within X . Therefore, the 1-D convolution layer applies its filters across a window of time steps, considering all V channels within that window to compute its output features. The notation $h^{(0)}$ used in the description below simply refers to this initial $T \times V$ input tensor X before any convolutional transformations are applied.

The encoder is structured as a series of convolutional layers, designed to extract meaningful features from the input molecular representation. Each subsequent convolutional layer increases in both depth (number of filters per layer) and width (size of each kernel) according to growth factors (optimized to 1.16), enabling the network to capture increasingly complex molecular features at different scales for learning hierarchical representations of molecular structures. More formally, the input $h^{(0)}$ (as layer 0) first passes through a sequence of four one-dimensional convolutional layers ($j = 1 \dots 3$).

The kernel sizes are chosen to capture common, local chemical motifs within that span such as aromatic rings and functional groups of the SMILES sequence (layer 1: 9 filters, kernel size 9, layer 2: 9 filters, kernel size 9, layer 3: 10 filters, kernel size 11). Subsequent layers progressively increase the number of filters by a geometric factor, allowing the network to learn a richer hierarchy of features by combining simpler patterns, while the stacking of layers increases the effective receptive field to capture longer-range dependencies. Each layer applies the convolution operation (although implemented as cross-correlation in Keras because flipping the kernel is an unnecessary computational step when the kernel's weights are learned during training) on the previous layer's output as follows

$$h_{\text{conv}}^{(j)} = \tanh(W_{\text{conv}}^{(j)} * h^{(j-1)} + b_{\text{conv}}^{(j)}), \quad (3)$$

using a hyperbolic tangent activation, followed by batch normalization

$$h_{\text{norm}}^{(j)} = \text{BatchNorm}(h_{\text{conv}}^{(j)}) = \gamma^{(j)} \frac{h_{\text{conv}}^{(j)} - \mu_{\beta}}{\sqrt{\sigma_{\beta}^2 + \epsilon}} + \beta^{(j)}, \quad (4)$$

to stabilize training. Here μ_{β} is the mini-batch mean, σ_{β}^2 is the mini-batch variance, ϵ is a small constant added to the variance for numerical stability (10^{-5}) to prevent division by zero in case the mini-batch variance is zero, $\gamma^{(j)}$ is a learnable scaling parameter allowing the network to adjust the variance of the normalized activations, and $\beta^{(j)}$ is a learnable shifting parameter that allows the network to adjust the mean of the normalized activations. Batch normalization was applied after each convolutional layer to improve generalization by normalizing the inputs to each layer.

The output tensor from the final convolutional layer is flattened into a vector $h^{(4)}$. This vector is processed by a single dense layer employing tanh activation and batch normalization, with dropout applied, allowing for mixing of the extracted convolutional features. Let the output of this layer be denoted h_{enc} , which represents a compressed encoding of the input SMILES sequence.

The parameters of the latent Gaussian distribution $q_{\phi}(z|X) \sim \mathcal{N}(\mu_{\phi}, \sigma_{\phi}^2 I)$ are then derived from this intermediate encoding h_{enc} in two distinct steps, handled by different parts of the model structure:

1. **Latent mean (μ) vector calculation:** The main encoder function computes the latent mean vector μ by applying a dense layer with a linear activation function directly to the intermediate encoding h_{enc}

$$\mu_{\phi} = W_{\mu} h_{\text{enc}} + b_{\mu}. \quad (5)$$

The encoder model function returns both this calculated mean μ and the intermediate encoding h_{enc} .

2. **Latent log-variance ($\log \sigma^2$) vector calculation:** A separate function also takes the intermediate encoding h_{enc} as input. It then applies a separate dense layer with a linear activation function, to h_{enc} to compute the latent log-variance vector $\log \sigma_{\phi}^2$

$$\log \sigma_{\phi}^2 = W_{\sigma^2} h_{\text{enc}} + b_{\sigma^2}. \quad (6)$$

To enable loss gradient backpropagation through the sampling process a reparameterization trick expresses the latent vector z as a deterministic function of the learned mean μ_{ϕ} , log-variance $\log \sigma_{\phi}^2$ and independent standard Gaussian noise, ϵ [16]. Specifically, z is computed as $z = \mu_{\phi} + \exp(0.5 \log \sigma_{\phi}^2) \odot \epsilon$, where $\epsilon \sim \mathcal{N}(0, I)$. This isolates the randomness in ϵ , allowing gradients to flow from the VAE loss back to the encoder parameters μ and $\log \sigma^2$ for end-to-end training.

The dimensionality of the latent space, D , defines the capacity of the variational bottleneck. This separation allows the main encoder model structure to focus on producing the mean and the feature representation, while the dedicated variational layers function handles the variance prediction and the sampling process.

VAE latent space: The encoder network, parameterized by ϕ , maps an input SMILES token sequence X onto a probabilistic representation in the latent space. Specifically, it outputs the parameters of an approximate posterior distribution $q_\phi(z|X)$ as a multivariate Gaussian with a diagonal covariance matrix

$$q_\phi(z|X) = \mathcal{N}(z|\mu_\phi(X), \text{diag}[\sigma_\phi^2(X)]). \quad (7)$$

Here, $z \in \mathbb{R}^D$ is the latent vector corresponding to the input X governed by $q_\phi(z|X)$, which defines the location and spread in the D -dimensional latent space. Therefore, instead of a deterministic point, multiple latent vectors z may be obtained for each SMILES X by sampling from this distribution.

VAE decoder: The decoder network reconstructs the SMILES sequence from a single sampled latent vector $z \in \mathbb{R}^D$. The sampled vector first passes through a single dense transformation layer. This layer employs a hyperbolic tangent (tanh) activation function followed by batch normalization, to prepare the latent representation for sequential processing

$$h_{\text{dec}}^{(1)} = \text{BatchNorm}(\tanh(W_{\text{dec}}^{(1)} z + b_{\text{dec}}^{(1)})), \quad (8)$$

with dropout applied. The resulting vector $h_{\text{dec}}^{(1)}$ is then replicated T times (the maximum sequence length) using a repeat vector operation, creating an input sequence $H_{\text{repeat}} = [h_{\text{dec}}^{(1)}, h_{\text{dec}}^{(1)}, \dots, h_{\text{dec}}^{(1)}]$ for the recurrent part of the decoder.

This sequence is processed by a stack of three standard Gated Recurrent Units (GRUs) ($k = 1, 2, 3$), chosen for their effectiveness in capturing temporal dependencies while mitigating vanishing gradient issues. Each standard GRU layer k computes its hidden state, $h_t^{(k)} \in \mathbb{R}^{488}$, based on the previous hidden state, $h_{t-1}^{(k)}$, and the output, $h_t^{(k-1)}$ from the layer below ($h_t^{(0)}$ being the t -th vector from H_{repeat}).

The GRU update equations are standard:

$$r_t^{(k)} = \sigma_g(W_r^{(k)} h_t^{(k-1)} + U_r^{(k)} h_{t-1}^{(k)} + b_r^{(k)}), \quad (9a)$$

$$u_t^{(k)} = \sigma_g(W_u^{(k)} h_t^{(k-1)} + U_u^{(k)} h_{t-1}^{(k)} + b_u^{(k)}), \quad (9b)$$

$$\tilde{h}_t^{(k)} = \tanh(W_h^{(k)} h_t^{(k-1)} + U_h^{(k)} (r_t^{(k)} \odot h_{t-1}^{(k)}) + b_h^{(k)}), \quad (9c)$$

$$h_t^{(k)} = (1 - u_t^{(k)}) \odot h_{t-1}^{(k)} + u_t^{(k)} \odot \tilde{h}_t^{(k)}, \quad (9d)$$

where σ_g is the sigmoid function, \tanh is the internal activation and \odot is element-wise multiplication. Stacking GRUs allows the decoder to model increasingly complex temporal patterns necessary for generating syntactically valid SMILES sequences.

The final layer ($k = 4$) is a custom Terminal GRU (TGRU) layer designed to leverage teacher forcing during training. In this mode, the TGRU's state update incorporates the true previous token from the input sequence, x_{t-1}^{true} (the one-hot vector for the ground truth character at step $t-1$), in addition to the input from the layer below ($h_t^{(3)}$) and its own previous hidden state ($h_{t-1}^{(4)}$). Specifically, the candidate hidden state $\tilde{h}_t^{(4)}$ calculation is modified to include a term dependent on the true previous input, gated by the reset gate $r_t^{(4)}$

$$\tilde{h}_t^{(4)} = \tanh(W_h^{(4)} h_t^{(3)} + r_t^{(4)} \odot (U_h^{(4)} h_{t-1}^{(4)} + U_x^{(4)} x_{t-1}^{\text{true}}) + b_h^{(4)}), \quad (10)$$

where $U_x^{(4)}$ represents the weights applied specifically to the teacher-forced input x_{t-1}^{true} . This teacher forcing mechanism provides the network with the correct preceding character during training, which can stabilize learning and accelerate convergence for sequence generation tasks.

This resulting hidden state $h_t^{(4)}$ from the TGRU encapsulates the information needed to predict the probability distribution for the next token. It is projected to the vocabulary dimension via a final dense (fully connected) layer to produce raw, unnormalized scores (logits) $o_t \in \mathbb{R}^V$: $o_t = W_{\text{out}} h_t^{(4)} + b_{\text{out}}$, where W_{out} and b_{out} are the learnable weight matrix and bias vector of this final dense layer. These logits are then passed through a softmax activation function, moderated by a temperature τ , to yield the reconstructed probability distribution vector \hat{X}_t over the vocabulary V for the token at time step t

$$\hat{X}_{t,i} = \frac{\exp(o_{t,i}/\tau)}{\sum_{k'=1}^V \exp(o_{t,k'}/\tau)}, \quad (11)$$

where $\hat{X}_{t,i}$ is the i -th element of the vector \hat{X}_t , representing the probability assigned to the i -th vocabulary character at time step t . The temperature parameter τ specifically modifies the character sampling process used during sequence generation (e.g., at test time), adjusting the trade-off between exploiting high-probability tokens (lower τ) and exploring more diverse options (higher τ). The default value $\tau = 1.0$ results in sampling based on the unmodified output probabilities during generation.

Odor prediction head: For any decoded SMILES token sequence the combined model features a dedicated property prediction head that takes the latent vector z as input. This regression head begins with a dense layer compressing the latent representation for the decoded molecule into a 36-dimensional space, initiating a processing pathway focused on property feature prediction. Two additional dense layers are applied allowing for hierarchical feature extraction. The dimensionality progressively decreases through these layers, with each subsequent layer having 80% of the units of the previous one to distill property-relevant information efficiently. Batch normalization is applied after each intermediate layer, which helps stabilize training dynamics and dropout is applied to improve generalization. The network culminates in a specialized output layer: one employing a linear activation function to predict continuous values suitable for regression tasks (optimized using Mean Squared Error – see Section below). The final layer of the odor prediction head has a single output representing $P(\text{odor})$ property prediction for any decoded molecule.

Model training

The combined VAE-QSAR model is trained end-to-end by optimizing the parameters of the encoder (ϕ), odor prediction head and decoder (θ) to maximize the Evidence Lower Bound (ELBO) on the marginal log-likelihood of the data $\log p(X)$. This is equivalent to minimizing the negative ELBO, which serves as the primary loss function. The loss function \mathcal{L}_{VAE} for a single input sequence X is composed of three terms: a reconstruction loss, a Kullback-Leibler (KL) divergence regularization term and an odor property prediction loss.

$$\mathcal{L}_{\text{VAE}}(X, \theta, \phi) := \underbrace{\beta_{KL}(e) \cdot D_{KL}(q_\phi(z|X) \| p(z))}_{\text{Regularization (KL Divergence)}} + \underbrace{\mathcal{L}_{\text{recon}}}_{\text{Reconstruction Loss}} + \underbrace{\gamma \mathcal{L}_{P(\text{odor})}}_{\text{Property Prediction Loss}} \quad (12)$$

Here, $q_\phi(z|X)$ is the approximate posterior distribution $\mathcal{N}(z|\mu_\phi(X), \text{diag}[\sigma_\phi^2(X)])$ parameterized by the encoder's outputs $(\mu_\phi, \log \sigma_\phi^2)$, $p_\theta(X|z)$ is the likelihood of the data given the latent variable parameterized by the decoder, and $p(z)$ is the prior distribution over the latent variables, chosen as a standard multivariate Gaussian $\mathcal{N}(z|0, I)$.

The reconstruction loss, $\mathcal{L}_{\text{recon}}$, measures how accurately the decoder reconstructs the input using the latent representation of X alone. Given the categorical nature of SMILES tokens and the decoder's softmax output $\hat{X}_{t,i} = p_\theta(X_t = i|z)$, this term is implemented as the categorical cross-entropy, summed over the sequence length T and vocabulary size V

$$\mathcal{L}_{\text{recon}} := - \sum_{t=1}^T \sum_{i=1}^V X_{t,i} \log(\hat{X}_{t,i}). \quad (13)$$

The base weight for this reconstruction term is set to $w_{\text{xent}} = 1.0$.

The KL divergence term acts as a regularizer, encouraging the approximate posterior $q_\phi(z|X)$ to stay close to the prior $p(z)$. For the chosen Gaussian distribution, it has an analytical form calculated over the latent dimension

$$D_{KL}(q_\phi(z|X) \| p(z)) = \frac{1}{2} \sum_{j=1}^D (\sigma_{\phi,j}^2 + \mu_{\phi,j}^2 - 1 - \log \sigma_{\phi,j}^2). \quad (14)$$

The weight $\beta_{KL}(e)$ applied to the KL divergence term is annealed during training scheduled over epoch e . This annealing begins with the KL weight near zero and gradually increases it, allowing the model to initially focus on achieving good reconstruction before strongly enforcing the latent space structure. The annealing follows a cyclical schedule centered at epoch $e_{\text{start}} = 22$ with a slope $s = 1.0$, scaled by a target KL weight $\beta_{\text{target}} = 1$

$$\beta_{KL}(e) = \beta_{\text{target}} \frac{1}{1 + \exp(-s(e - e_{\text{start}}))}. \quad (15)$$

This annealing strategy helps prevent the KL term from collapsing the latent space prematurely ("posterior collapse").

The overall loss, averaged over a mini-batch of size B , is minimized using the Adam optimizer. Adam is chosen for its adaptive learning rate capabilities, with a learning rate $\eta = 3.12 \times 10^{-4}$ and a first moment estimate decay factor $\beta_1 = 0.937$. To ensure the robustness of the generative framework, we performed a systematic grid search across the key architectural and optimization hyperparameters using the candidate values listed in Table 1. The final configuration (highlighted in bold) was selected based on performance metrics evaluated on the validation set, specifically prioritizing parameter combinations that minimized the overall ELBO loss while maintaining stable convergence and high reconstruction accuracy. Training was performed for a specified number of epochs using 10% (validation split = 0.1) of the data for validation to monitor generalization and prevent overfitting. The entire training procedure aims to find model parameters (θ, ϕ) that yield both accurate reconstructions and a well-structured latent space adhering to the Gaussian prior. The odor prediction head is trained

Table 1. Hyperparameter Optimization Search Space. The optimal values selected for the final VAE-QSAR model are highlighted in **bold**.

Hyperparameter	Values Evaluated				
Latent Space Dimensions (D)	64	128	196	256	512
GRU Hidden Units	128	488	512	768	1024
Convolutional Growth Factor	1.00	1.10	1.12	1.16	1.25
Learning Rate (η)	1.0×10^{-3}	5.0×10^{-4}	3.12×10^{-4}	1.0×10^{-4}	1.0×10^{-5}
Adam Optimizer Decay (β_1)	0.900	0.925	0.937	0.950	0.990
Batch Size (B)	32	64	100	128	256
KL Annealing Center (e_{start})	10	15	22	30	50
Odor Head Compression Ratio	0.50	0.65	0.75	0.80	0.90
CNN Kernel Size (Layer 1)	3	5	7	9	11
Softmax Temperature (τ)	0.5	0.8	1.0	1.2	1.5

using the probability of the corresponding molecule being odorous according to the QSAR model, $P(\text{qsar})$, following a mean-square loss (MSE) criterion over a mini-batch (see Section 2.4 below on the QSAR logistic regression model used to generate these targets). For a single SMILES sequence

$$\mathcal{L}_{\mathcal{P}(\text{odor})} := [P(\text{qsar}) - P(\text{odor})]^2. \quad (16)$$

During training, the contribution of the autoencoder multiple objectives is configured by default to be balanced equally. Balancing these multiple objectives means that the VAE’s latent space possesses several key properties for encoding molecular structures. The space is shaped by regularization and smoothness constraints imposed by the KL divergence term in the VAE objective. This term encourages the learned distributions $q_\phi(z|X)$ to stay close to a prior $p(z)$, forcing encodings into a structured region and promoting continuity where similar molecules map to nearby, overlapping distributions, enabling meaningful interpolation for molecular generation. Lastly, the dimensionality (optimization settled on $D = 196$) of the latent space controls the balance between compactness and expressiveness. It dictates the number of dimensions available to capture molecular variations, with smaller D promoting efficiency but potentially limiting detail, while larger D allows richer representation but requires sufficient regularization to remain meaningful.

The batch size $B = 100$ was found to balance computational efficiency and the stochasticity needed for effective training. The number of training epochs is determined based on convergence and acceptable validation set overall loss. The encoder’s convolutional stack along with subsequent layers that further expand geometrically using these factors, aims to capture diverse local chemical motifs and progressively build hierarchical features with an increasing receptive field. Standard stride 1 and ‘valid’ padding are used within the CNN layers. The recurrent component employs four GRU layers, each with a recurrent dimension of 488, found to adequately model sequential dependencies in SMILES strings without being computationally prohibitive. Training used the Adam optimizer, selected for its adaptive capabilities, optimised to a learning rate $\eta = 3.12 \times 10^{-4}$ and $\beta_1 = 0.937$. Overall, these parameters were found to capture hierarchical sequence features accurately, learning a structured latent space via controlled regularization, and achieving stable convergence.

QSAR odor prediction model

Molecular descriptors $m^{(i)}$ for each molecule i were calculated using Mordred descriptor calculator [16] covering a wide set of properties (Figure 2a). Both 2-D and 3-D descriptors were used, resulting in a total of 1,828 molecular features. Descriptors that generated non-numeric results for at least one training set molecule were discarded. Highly correlated ($\rho > 0.99$) descriptors were removed. Descriptors with low variance across the data-set ($\sigma^2 < 0.05$ after autoscaling) were also removed, resulting in 811 remaining descriptors used for the analysis. SMOTE algorithm was used to solve class imbalance by oversampling the data-set resulting in $n = 1,615$ for both classes [17].

To generate the targets for the odor prediction head of the VAE we trained a logistic regression model on a previously validated set of 1,615 odor and 309 non-odor molecules [14].

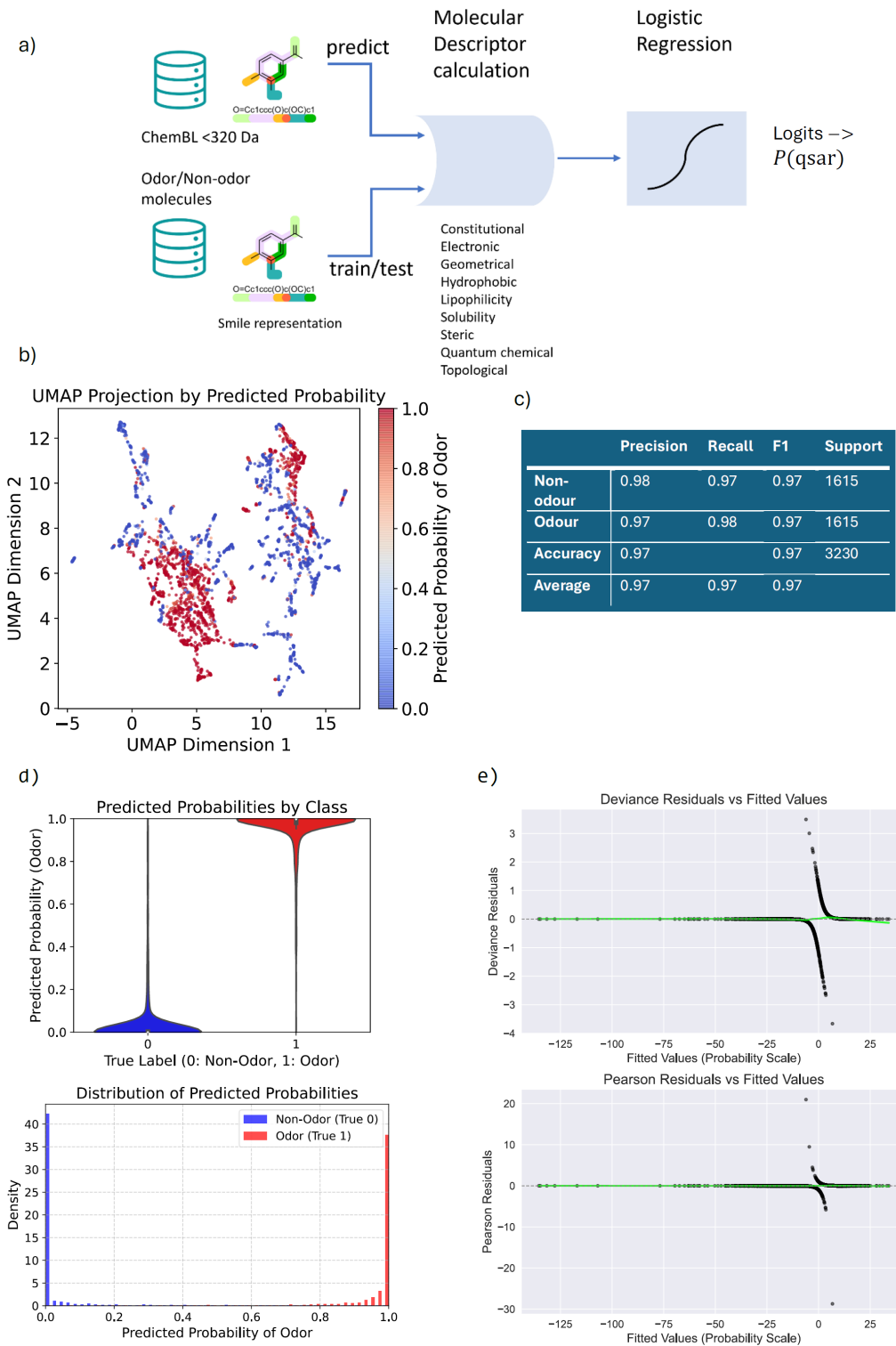


Figure 2. QSAR Odor molecule prediction results. a) Schematic showing the QSAR model pipeline where logistic regression was trained on 1,924 experimentally validated and/or literature reported molecules and subsequently used to label ChemBL molecules with a target odor probability, b) UMAP visualization of training set in space of molecular descriptors showing the odor probability, c) classifier performance for logistic model, and d) Distribution of predicted probabilities across the training set, and e) residual plots for the logistic regression model.

For a vector of molecular descriptors $m^{(i)}$ corresponding to a given molecule i , we used a logistic regression model that describes the probability of this molecule being odorous in terms of a single binary-dependent variable $y^{(i)}$

$$P(\text{qsar}) = P(y^{(i)} = 1 | m^{(i)}) = f_{\theta}(m^{(i)}) = \frac{1}{1 + e^{-\theta^T m^{(i)}}}, \quad (17)$$

where θ denotes the parameter vector to be learnt (often termed logistic regression beta coefficients) across all molecular descriptors. To optimize this, we minimize the logistic loss (negative log-likelihood) cost function over a training set of n molecules, which is equivalent to maximizing the likelihood of observing the given data under the logistic regression model

$$J(\theta) = -\frac{1}{n} \sum_{i=1}^n [y^{(i)} \log(f_{\theta}(m^{(i)})) + (1 - y^{(i)}) \log(1 - f_{\theta}(m^{(i)}))], \quad (18)$$

where $y^{(i)}$ is the class label (0 non-odor and 1 odor) and $m^{(i)}$ is the feature vector for the i^{th} training example (molecule in training set).

Loss minimization is performed using gradient descent with the following update rule for each parameter within θ

$$\theta_j := \theta_j - \alpha \frac{1}{n} \sum_{i=1}^n (f_{\theta}(m^{(i)}) - y^{(i)}) m_j^{(i)}, \quad (19)$$

where α is the learning rate. Cross-validation was used to avoid overfitting the training set and check model performance on unseen molecules.

Results

Odor prediction QSAR model validation

Logistic regression model fitting to the QSAR molecule training set resulted in precision, recall and $F1 = 0.97$ (Figure 2c - cross-validated to 10-fold). Overall accuracy was 97%. Predicted odor probabilities separated adequately showing acceptable error for use in subsequent training of the VAE (mean probability for non-odor class = 0.043, odor class = 0.957, Figure 2d). UMAP was used on the 811 descriptors for dimensionality reduction and visualization of predicted probabilities in the molecular descriptor space (Figure 2b).

Dep. Variable:	odor.class
No. Observations	3230
Model	Logit
Df Residuals	2858
Method	MLE
Df Model	371
Pseudo R ²	0.894
Log-Likelihood	-235.80
LL-Null	-2238.9
LLR p-value	0.000

Table 2. Logistic Regression Model Diagnostics

After fitting the logistic function, diagnostics and classification performance were checked (Table 2). Logistic regression is based on the following assumptions that were tested on the fitted model [18]:

1. Binary response variable: Logistic regression assumes that the response variable has only two possible outcomes – verified odor and non-odor molecules were applied in the training set so only dichotomous training data were considered.
2. Independence of errors: Logistic regression assumes that errors (residuals) are independent. Figure 2e shows the residual errors for the training set in the original and Pearson standardized coordinates have no repeat error values (monotonic).
3. Observations are independent: Logistic regression requires that the observations be independent of each other, meaning they should not come from repeated measurements or matched data. As each molecule is separately sampled across a random set of training molecules, observations can be considered independent.

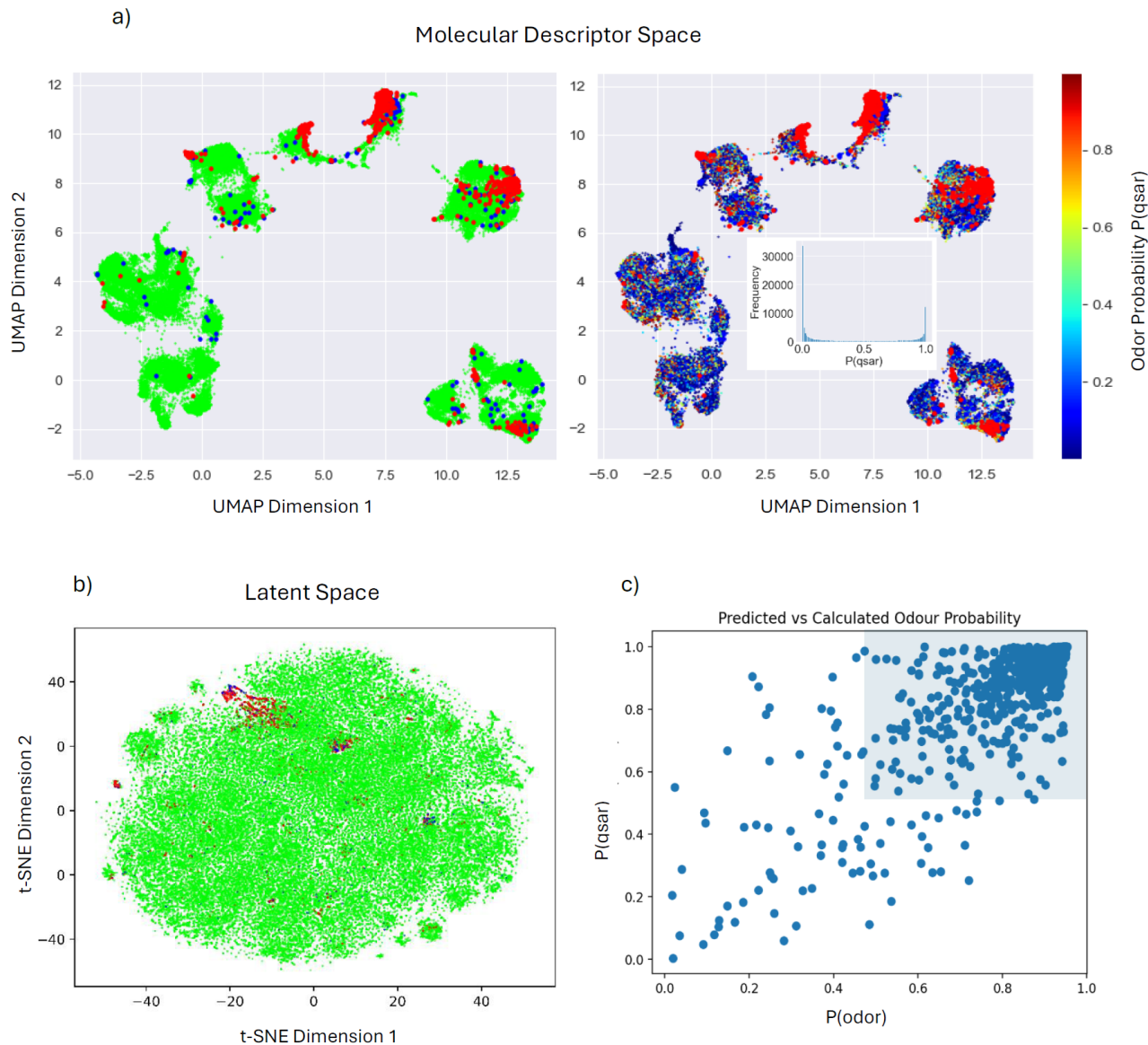


Figure 3. a) UMAP dimensionality reduction and visualization of the molecular descriptor space showing $\sim 5 \times 10^5$ VAE training set ChemBL molecules (green) alongside the original set of odor molecules (red) and non-odor molecules (blue) and the same UMAP representation showing the predicted probabilities across all ChemBL molecules used for VAE training as predicted by the QSAR model (right). Inset histogram for the frequency of odor probabilities in the ChemBL set used to train the VAE, b) t-SNE dimensionality reduction of 1×10^4 randomly sampled ChemBL molecules encoded into the latent space (green) together with validated odor (red) and non-odor molecules (blue), c) Validated odor molecule probabilities as predicted by the QSAR model, $P(\text{qsar})$, compared against VAE odor property prediction, $P(\text{odor})$. Shaded region shows where both models agree on odor molecule prediction ($P(\text{odor}) > 0.5$ and $P(\text{qsar}) > 0.5$).

4. No multicollinearity: Logistic regression requires that the independent variables are not too highly correlated with each other. This is ensured by removing highly correlated molecular descriptors before logistic regression is applied.

The rank order of the absolute model coefficient values showing the contribution of each Mordred molecular descriptor to predicting odor probability is shown in Figure S1 (descriptor names can be resolved from [19]).



Figure 4. Generated molecules from four example seed odor molecules. a & b) Two example seed molecules (seed is distance 0.0, top left) with sampling of the latent space over increasing distance from the seed in latent space (units of $\sigma_\phi(z|X)$). Where available Pubchem catalogued compounds show their corresponding IUPAC name and CID reference, whereas potentially novel compounds show the corresponding SMILES and CID: N/A. SA: synthesis accessibility score. c) traversing the latent space between two odor seed molecules $t = 0$ is start seed and $t = 1$ is the end seed in 11 discrete steps. Attempts are the number of probabilistic decode cycles required to obtain a valid structure at that point of the latent space.

VAE training with ChemBL molecules

To provide a sufficiently large set of molecules for VAE training, the fitted QSAR model was applied to a random sample of $\sim 5 \times 10^5$ compounds (< 320 Da) from ChemBL [20] to predict their probability of odor, $P(\text{qsar})$. The molecular descriptor space was then visualized using UMAP against the original QSAR validated odor/non-odor set (Figure 3a). ChemBL molecules were chosen due to bioactive properties but also a low occurrence of odor molecules - to specifically test the hypothesis that the final generated molecules still retain odor characteristics in contrast to the training set (see histogram inset Figure 3a, right). Importantly, the validated odor/non-odor molecule set was not used to train the VAE directly, but rather via ChemBL to provide sufficient examples to learn the SMILES grammar itself and QSAR model generated target probabilities.

After training the VAE on the ChemBL molecule set we examined their representation within the 196-dimensional latent space (Figure 3b) using t-SNE and plotted them alongside the original odor/non-odor molecule set. With some exceptions, QSAR training set odor compounds (red) were found to cluster within the overall latent space distinct from the non-odor and ChemBL molecules. This suggests that the multi-task loss function is effective in organizing the latent space representation by odor properties even though the VAE was not trained on the QSAR training odor molecule set directly.

To check the fidelity of the knowledge distillation process from QSAR to VAE models, we compared the $P(\text{odor})$ values from the VAE odor prediction head against the corresponding QSAR model predicted values, $P(\text{qsar})$ (Figure 3c) using the original training set. The shaded region shows classification agreement between the two models, yielding a precision of 0.98, a recall of 0.97, and an F1-score of 0.97. This high agreement confirms that the VAE successfully captured the QSAR model's decision boundary and encoded the supervisory signal into its latent space. However, as the QSAR model serves as the training objective, this agreement represents internal consistency rather than external biological validation that comes later. The rigorous test of the model's ability to generalize to true olfactory biology is presented in subsequent sections using the external 'Unique Good Scents' dataset, which was unseen by both the QSAR and VAE components.

Generative molecule resampling from the latent space

Because the VAE maps SMILES onto a probability distribution with mean and log variance within the latent space, $q_\phi(z|X)$, resampling is possible to generate closely related decoded molecules.

To generate new molecules near a known seed molecule in the latent space, the VAE's encoder first predicts the mean latent representation (μ_{seed}) from the corresponding seed SMILES tensor X_{seed} , which is then standardized using the global mean (μ_{global}) and standard deviation (σ_{global} ; both of which are computed across the training set's latent space distribution during training), such that $z_{\text{seed}} = (\mu_{\text{seed}} - \mu_{\text{global}})/\sigma_{\text{global}}$. To explore the latent space around this standardized point, a resampling process adds controlled noise. Briefly, a noise vector (ϵ_{noise}) is sampled from a standard multivariate normal distribution $\mathcal{N}(0, I)$, normalized to unit magnitude, $\hat{\epsilon}_{\text{noise}}$, and then scaled by a specified scalar distance parameter, d , which dictates the Euclidean distance of the perturbation in the latent space. This scaled noise vector ($\delta z = d\hat{\epsilon}_{\text{noise}}$) is added to the standardized latent seed point: $z_{\text{perturbed}} = z_{\text{seed}} + \delta z$. Before this perturbed vector can be processed by the decoder, it must be unstandardized back to the original scale of the latent space using the inverse transformation: $z_{\text{dec}} = z_{\text{perturbed}} \odot \sigma_{\text{global}} + \mu_{\text{global}}$. Finally, the decoder network takes this resulting unstandardized vector as input and translates it into a new candidate SMILES string X_{gen} . To ensure the production of physically interpretable structures, a rejection sampling strategy was employed. If the decoded SMILES sequence failed syntax validation checks (via RDKit), the decoding process was repeated probabilistically for that latent point until a valid structure was obtained or a maximum retry limit was reached (see Figure 4c for attempt counts)

To test whether the odor properties of generated molecules are locally related in latent space we then applied as input the QSAR training set as seed molecules to the combined model and resampled the latent space at varying distances from the seeds (Figure 4a,b). To assess their odor likelihood we then ran these generated molecules through the fitted QSAR model. The majority of generated molecules are found to have $P(\text{qsar})$ and $P(\text{odor}) > 0.9$ (Figures 4, 6b(inset) and Supplementary Information). SMILES sequence validity was checked using standard RDKit syntax check and sanitization (chemical plausibility check).

Molecular VAE encoding capacity

The calculated average pairwise Euclidean distance between seed molecules in the latent space of 2.67 ± 0.79 (units of $\sigma_\phi(z|X)$) provides a quantitative measure of the encoding capacity of the combined model when compared with distances of generated molecules (Figure 4a,b). The inter-seed distance compared against the distances of resampled points in the latent space shows at least one order of magnitude encoding capacity greater than seed compounds originally used for training, which is essential for discovering novel chemical entities. Depending on search distances explored from seeds we found each run generates between 20 – 50k unique molecules indicating an encoding capacity of at least 10 - 25 times multiplier on the seed odor set.

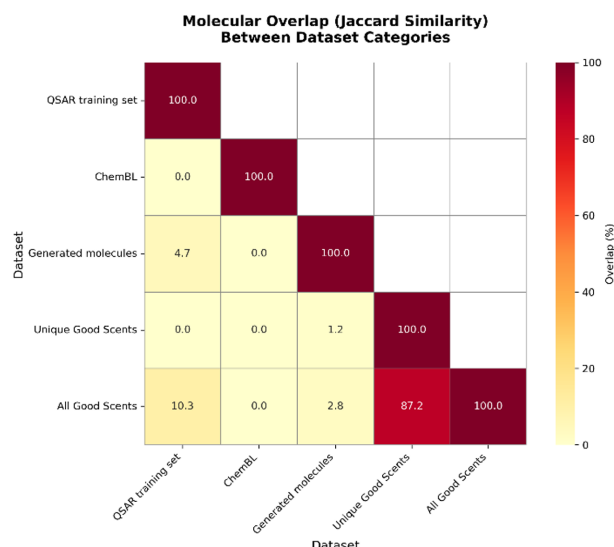
As a follow-up study, generated molecules and their corresponding $P(\text{qsar})$ values could be reintroduced for self-supervised training to further improve the encoding capacity of the combined model and more fully explore the latent space embeddings.

Molecular diversity and odor relevance

The generated molecules are found to contain diverse structural features and functional groups known to be important in odor and flavors and many compounds belong to multiple categories (Supplementary Information)

- Aromatic compounds: many molecules contain benzene rings, indicated by notations like 'c1ccccc1'. Examples include benzaldehyde ('O=Cc1ccccc1') and various substituted benzenes.
- Aldehydes: molecules with the 'C=O' group, such as 'O=Cc1ccccc1'.
- Carboxylic acids: compounds ending with 'C(=O)O', such as 'CC(=O)O'.
- Ketones: containing a carbonyl group between carbon atoms, e.g., 'CC(=O)CC(C)C'.
- Alcohols: compounds containing the '-OH' group, such as 'CC(=O)CC(C)O'.
- Amines: molecules with nitrogen atoms, like 'CN1CNC2CCCCC12'.
- Heterocyclic compounds: cyclic structures containing atoms other than carbon, e.g., 'CC1CNC2SCCCC12'.
- Alkenes: molecules with carbon-carbon double bonds, like 'C=C(C)C'.
- Halogenated compounds: molecules containing halogens (F, Cl, Br), such as 'CCC(C)F'.
- Sulfur-containing compounds: molecules with sulfur atoms, e.g., 'C=CCNSC=C'.
- Esters: compounds with the 'COC=O' group, like 'CC(=O)OC(C)C'.
- Nitriles: molecules containing the 'C#N' group, such as 'N#Cc1ccccc1'.
- Ethers: compounds with the 'C-O-C' linkage, e.g., 'COCCCCOCC'.
- Thiols and sulfides: molecules containing 'S-H' or 'C-S-C' groups, like 'CSCCS'.
- Phosphorus-containing compounds: molecules with phosphorus atoms, e.g. 'O=P(Cl)OCc1ccccc1'.
- Terpenes and terpenoids: complex molecules often found in essential oils, like 'CC(C)=CCCC(C)(O)C1CC=C(C)CC1'.

a)



b)

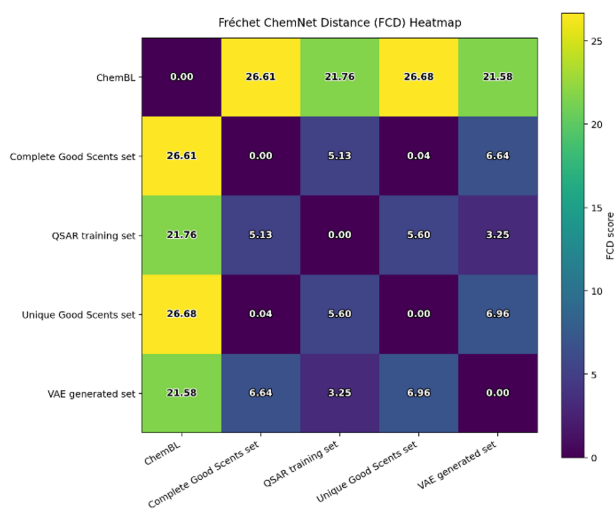


Figure 5. Generated molecules' uniqueness. a) Jaccard similarity, and b) Frechet ChemNET distance across data-sets.

Generated molecule uniqueness

As a check of generated molecule uniqueness we calculated the Jaccard similarity of the generated odor set against the QSAR model training set, ChemBL VAE training set and external Good Scents catalog of known odorants (Figure 5a)¹.

For validation purposes the Good Scents catalog was split into unique molecules that were unseen during both the QSAR model training and VAE ChemBL training phases. This ‘Unique Good Scents’ set serves as the primary external ground truth to validate that the QSAR-guided VAE has generalized to relevant chemical space beyond the limitations of the initial logistic regression teacher model. The generated set was found to contain no molecules from ChemBL and relatively few of the QSAR training set (4.7% Jaccard similarity). We also found a relatively low Jaccard similarity between the generated set and unique Good Scents molecules (1.2%), showing that the VAE was capable of discovering many new chemical structures without having seen them previously.

To evaluate the distributional fidelity of the generated chemical space, we calculated the Fréchet ChemNet Distance (FCD), a metric that quantifies the discrepancy between two molecular distributions based on internal activations of the ChemNet neural network [21]. Lower FCD scores indicate greater similarity in chemically and biologically relevant feature space. As shown in Figure 5b, the generated molecules exhibit a striking structural alignment with the known odorant manifold rather than the general chemical background they were trained on. Specifically, the generated set shows a high divergence from the ChemBL baseline ($FCD \approx 21.6$) but maintains a close proximity to the QSAR training set ($FCD \approx 3.25$). Notably, the distributional distance between the generated molecules and the external ‘Unique Good Scents’ catalog ($FCD \approx 6.96$) is comparable to the intrinsic variance observed between the two ground-truth odor datasets (Training vs. Unique Good Scents, $FCD \approx 5.60$). This confirms that the QSAR-guided loss successfully steered the VAE’s latent space away from the generic ChemBL distribution, producing a generative distribution that effectively mimics the structural diversity and feature density of verified odorants.

Table 3. Bemis-Murcko Scaffold Classification of Generated Molecules. The analysis distinguishes between memorization, derivatization of known structures, and the discovery of novel core frameworks. Average properties (Molecular Weight, LogP, and \log_{10} Vapor Pressure) indicate that even novel scaffolds maintain physicochemical profiles consistent with volatility.

Novelty Category	Count	% Gen.	MW	LogP	$\log_{10}(\text{VP})$	Interpretation
1. Exact Memorization	1020	5.34	142.81	2.14	2.54	Model memorized training data (Overfitting).
2. Odorant Derivatization (QSAR Scaffold)	3308	17.33	181.48	2.47	1.18	Optimizing side-chains of known odorant frameworks.
3. Repurposing (ChemBL Scaffold)	258	1.35	158.31	2.23	1.70	Converting generic bioactive frameworks into odorants.
4. Validated Scaffold Hop (Rediscovery)	294	1.54	153.27	2.01	2.61	True Generalization: Found known odorant frameworks not in training.
5. Uncharted Scaffold Hop (New IP)	14208	74.43	160.76	1.95	2.70	Novel frameworks. Potential new chemical entities.

Scaffold analysis and novelty depth

To rigorously assess whether the generated molecules represent true structural novelty or merely trivial derivatization (e.g., adding minor functional groups to known structures), we classified the generated set based on Bemis-Murcko scaffolds (Table 3). This method abstracts molecules to their core ring-linker frameworks, ignoring side chains. The analysis reveals that only 5.3% of generated molecules were exact matches to training data, while 17.3% represented derivatizations of known odorant scaffolds, effectively performing “lead optimization” by modifying side chains of validated olfactory cores. Crucially, 74.4% of the generated library falls into the “Uncharted Scaffold Hop” category, possessing core frameworks entirely absent from the training sets. These novel scaffolds exhibit physicochemical properties ideal for volatiles (Mean MW ≈ 160 Da, $\log_{10}(\text{VP}) \approx 2.70$), suggesting they represent plausible new chemical entities rather than generation artifacts. Furthermore, the model achieved a “Validated Scaffold Hop” rate of 1.5%, effectively rediscovering distinct odorant frameworks found in the external “Unique Good Scents” validation set that were never presented during training. This indicates the model has an ability to generalize structural rules of olfaction to discover valid, novel molecular architectures.

¹<https://www.thegoodsentscompany.com/allodor.html>

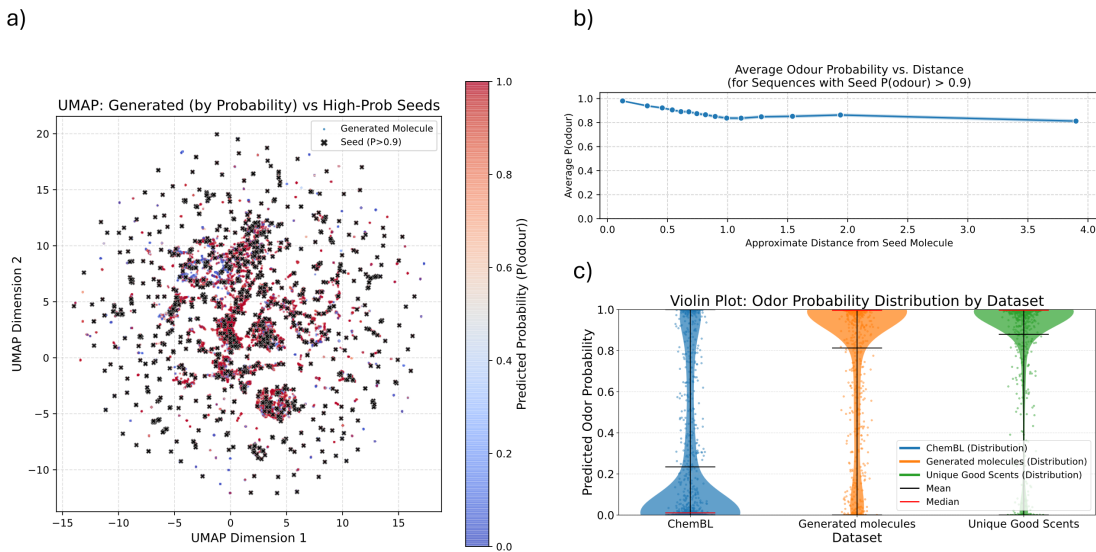


Figure 6. Generated molecules odour probability. a) UMAP representation of seed and generated molecules encoded in the latent space color-coded by odor (inset shows the $P(\text{qsar})$ distribution across all generated molecules). b) probability of generated molecule being odorous with distance from the seed (in units of $\sigma_\phi(z|X)$) averaged over all generated molecules (thickness shows 95% confidence interval). c) QSAR model predicted odour probabilities of random 1k molecules sampled from ChemBL, generated molecules set and unique Good Scents (ground truth compounds).

Latent space organization and structure-odor relationships

Generated compounds were found to vary continuously in odor likelihood with distance from a high probability odourant seed in the latent space (Figure 6a,b); however, sometimes small changes in the molecular structure could also dramatically change $P(\text{odor})$ (generative examples within Supplementary Information). Such discontinuities highlight the non-linear mapping between the continuous latent representation of molecular structure and the predicted biological property. This observation aligns with the concept of activity cliffs in structure-odor relationships (SORs), where minor chemical alterations can lead to significant perceptual shifts [22].

The latent space retains the smooth ‘chemical grammar’ necessary for generating valid molecules via interpolation (Figure 4 and Supplementary Information examples), while the integrated odor prediction capability reflects the sensitivity of olfactory perception to specific structural features. Running the generated molecule set through the QSAR model demonstrates that the distribution is distinct from the ChemBL grammar learning data-set whilst closer to the Unique Good Scents ground truth set (Figure 6c).

The finding that predicted odor probability drops only modestly on average (remaining > 0.8 even at significant distances from seed molecules) shows that the highest concentration of generated odors are within a close radius of a seed’s latent representation (Figure 6b), the persistence of elevated probability further out suggests the latent space is effectively organized by olfactory relevance. This implies that regions corresponding to odorous molecules are not isolated points but likely form continuous, potentially interconnected neighborhoods or manifolds within the latent space (Figure 5b shows a small increase in probability at the distance from the seed molecule close to that of neighboring seeds on average). As $P(\text{odor})$ remains relatively high over distances comparable to the average separation between known distinct odorants it reinforces the idea that the model can effectively bridge different regions of odor space. This result validates the utility of the multi-task learning approach, where the odor prediction loss actively guides the VAE to cluster odorants together. Practically, it means that sampling around known odorants is an effective strategy for discovering novel candidates that retain desirable olfactory properties, confirming the potential for guided exploration within the chemical space.

By adjusting the loss function coefficients (β_{KL}, γ in Equation 12) the framework allows for adjusting the trade-off between maintaining strict chemical continuity/similarity (grammar) and maximizing the desired odor property. This adjustability enables researchers to either perform broad exploration of chemically plausible space or focus generation efforts (‘exploitation’) specifically towards regions predicted to yield high odor probability, depending on the goals.

Generated molecule validity checks

To assess whether the generated SMILES sequences translate into physically realizable 3D entities, we subjected the *de novo* molecules to a battery of stringent validity checks (Table 4). Beyond standard syntactic correctness, which was enforced to

Table 4. Combined Validity, Energy, Structural, and Novelty Metric Checks

Dataset	Chemical Validity Checks			Geometric	Physical	Structural Alerts (PAINS)		Novelty / Overlap	
	RDKit Valid (%)	OpenBabel Valid (%)	Cross Valid (%)	Bredt Compliant (%)	Energy Strain Acceptable (%)	Clean / Free (%)	PAINS Alerts (%)	Unique (%)	Overlap (%)
Generated molecules	100.00	100.00	100.00	99.90	99.38	97.74	2.26	94.82	5.18
QSR Training Set	100.00	100.00	100.00	99.27	97.00	97.51	2.49	95.74	4.26
Unique Good Scents	100.00	100.00	100.00	96.85	99.60	99.24	0.76	99.08	0.92
All Good Scents	-	-	-	97.13	99.40	99.22	0.78	97.45	2.55
ChemBL	100.00	100.00	100.00	98.27	93.45	98.65	1.35	100.00	0.00

100.00% across both RDKit and OpenBabel parsers via rejection sampling, the generated candidates demonstrated exceptional geometric and physical plausibility. Notably, 99.90% of generated structures complied with Bredt's rule regarding double bond placement at bridgeheads—surpassing the compliance rates of both the training set (99.27%) and the general ChemBL baseline (98.27%). This structural integrity is further supported by energy strain calculations, where 99.38% of generated conformers fell within acceptable energy limits, aligning closely with the 'Unique Good Scents' ground truth. Furthermore, the model balanced structural novelty with medicinal chemistry viability; while 94.82% of the generated molecules were unique (novel entities), they maintained a low PAINS alert rate (2.26%) comparable to the QSAR training set (2.49%), indicating that the generative process explores new chemical space without introducing excessive structural liabilities or frequent assay interference artifacts.

Generated molecule physicochemical properties

The generated molecules exhibit physicochemical profiles that align closely with the established criteria for odorants, distinct from the broader chemical space represented by ChemBL (Figure 7). This comparison against the ChemBL baseline serves to validate that the model successfully targets the specific physicochemical niche of odorants, confirming the chemical relevance of the generated entities irrespective of the specific generative architecture employed. A critical determinant of olfactory perception is volatility; the generated molecules display a mean log vapor pressure of 1.66 Pa (calculated using *VaPoRs* [22], which is significantly higher than the non-odorant ChemBL baseline (-3.97 Pa) and comparable to the Unique Good Scents ground truth (0.26 Pa), ensuring sufficient volatility to reach the nasal epithelium [5]. Molecular weight analysis further corroborates this trend, with the generated set having a mean mass of 158.63 Da, effectively mirroring the lighter distribution of known odorants (186.79 Da) compared to the heavier ChemBL average (277.09 Da). This lower molecular mass is consistent with the requirement for rapid diffusion and receptor interaction [5] and the QSAR training set properties (generated molecules set mean MW= 158.62. \pm 53.47 Da vs. QSAR training set MW= 153.32. \pm 71.86 Da). In terms of hydrophobicity, the generated molecules possess a mean Log P of 1.67, falling well within the "Goldilocks" zone (typically 1–3) required for bioavailability and crossing the mucosal layer, whereas the ChemBL set extends into more lipophilic regions (mean 2.14). Structural complexity, measured by the number of rings and heteroatoms, also reflects the ground truth; generated molecules average 0.81 rings and 2.14 hydrogen bond acceptors, matching the Good Scents distribution (0.81 rings, 2.14 acceptors) far more closely than the ChemBL dataset (2.48 rings, 3.93 acceptors). The Kullback-Leibler divergence scores confirm this structural fidelity, showing minimal divergence between generated and ground truth distributions (e.g., Log P KL \approx 0.18) compared to the significant separation from ChemBL (Log P KL \approx 0.40).

Generated molecule safety

To assess the safety and suitability of the generated compounds for potential application, ADMET properties were predicted using ADMET-AI [23]. The generated set demonstrates a favorable safety profile with a low predicted probability of nuclear receptor toxicity. Specifically, the mean predicted activity for the Androgen Receptor (NR-AR) was 0.01, and for the Estrogen Receptor (NR-ER) was 0.07, values that are statistically indistinguishable from the Unique Good Scents catalog (NR-AR: 0.01; NR-ER: 0.09) and significantly lower than the ChemBL baseline (NR-AR: 0.02; NR-ER: 0.13). Mutagenicity potential, assessed via predicted Ames test outcomes, showed a mean probability of 0.30 for the generated molecules. While this is slightly elevated compared to the ground truth (0.14), it remains lower than the ChemBL background (0.36), suggesting that the generative process does not disproportionately introduce genotoxic structural alerts. Interestingly, the predicted probability of skin sensitization was higher in both the generated set (0.75) and the Good Scents collection (0.70) compared to ChemBL (0.52). This elevation likely reflects the reactive nature of many volatile organic compounds (such as aldehydes and enones) common in fragrance chemistry, highlighting a known trade-off between olfactory potency and potential dermal reactivity that requires standard regulatory management rather than indicating a failure of the generative model.

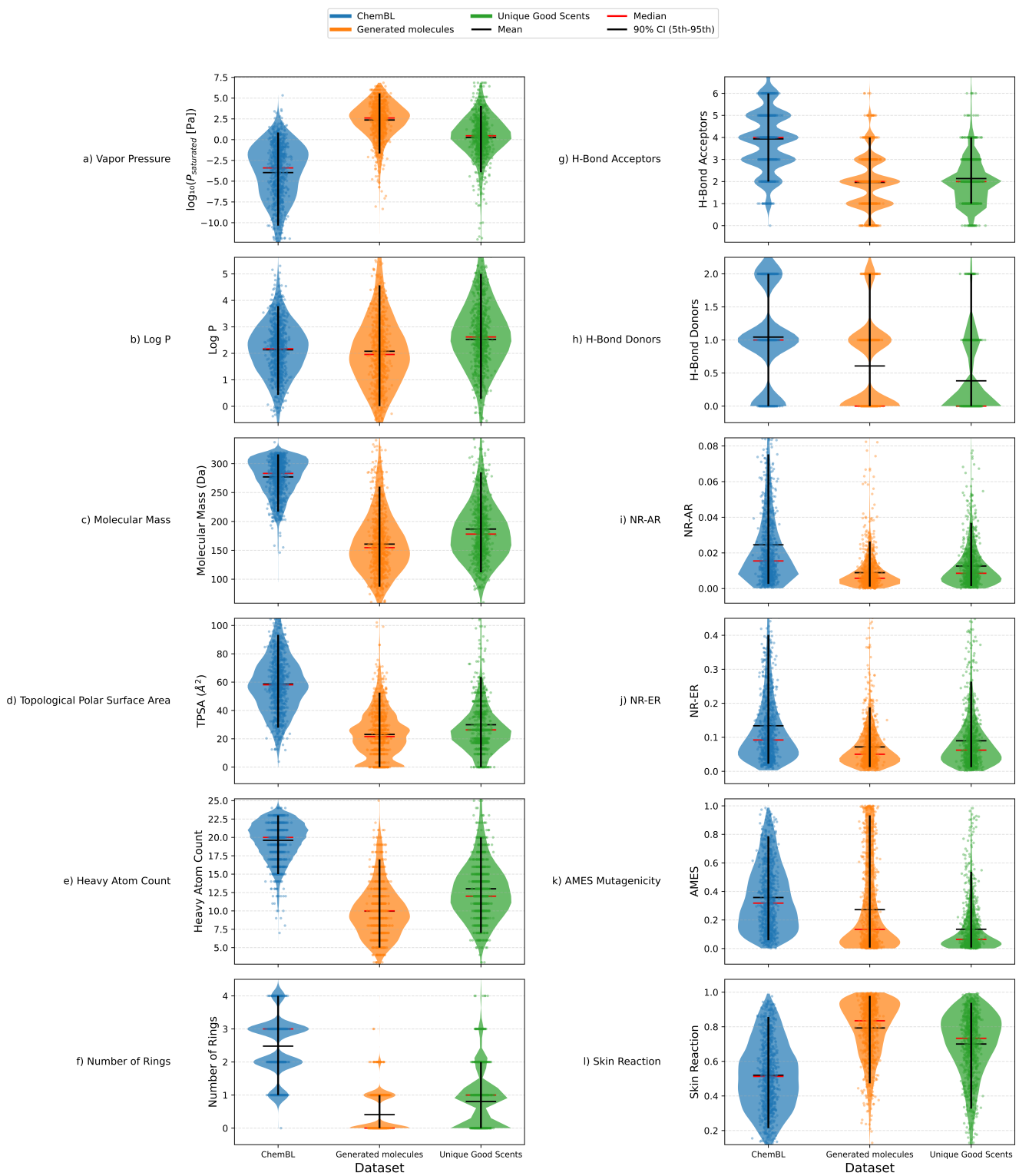


Figure 7. Physicochemical and ADMET property validation on generated molecules compared against ChemBL training molecules and unique Good Scents (ground truth compounds). a-h) Predicted physicochemical properties, i-l) Predicted ADMET properties, NR-AR: Nuclear Receptor – Androgen Receptor; NR-ER: Nuclear Receptor – Estrogen Receptor; Ames – Ames Mutagenicity Test; Skin Reaction.

Molecule synthesis accessibility

We also compared the synthesis accessibility (SA) for generated molecules by computing the SAScore using RDKit’s SAScorer (Figure 8a). This score is based on fragment contributions and includes a penalty for molecular complexity. While SA scores for generated compounds were found to be comparable to seed molecules, generated compounds have a slightly higher mean SA score of 3.01 ± 1.01 compared with seed molecules with mean SA score 2.51 ± 0.97 , possibly on account of increased diversity in the generated set and the fact that seed compounds are often optimized for their synthesis routes in the literature and public data-sets.

Data-set	% Solved	Avg state score	Min state score	Max state Score	State score st. dev.	Avg synth routes	Min synth routes	Max synth routes	Synth Routes st. dev	Avg reactions	Avg precursors	Avg precurs. in stock
Generated molecules	100.00	0.76	0.05	1.00	0.27	5.30	1.00	25.00	2.71	2.89	2.54	2.11
Unique Good Scents	100.00	0.92	0.05	1.00	0.17	4.10	1.00	16.00	2.31	1.85	1.99	1.71
ChemBL	100.00	0.90	0.05	1.00	0.15	4.85	1.00	21.00	2.50	2.65	2.67	1.71
All Good Scents	100.00	0.93	0.05	1.00	0.17	3.82	1.00	15.00	2.15	1.61	1.83	1.60

Table 5. Retrosynthesis analysis of data-sets

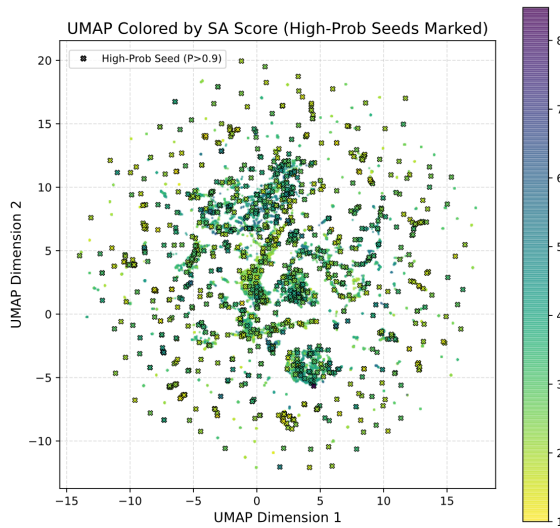
To move beyond theoretical validities and assess practical constructability, we performed a comprehensive retrosynthetic analysis using AiZynthFinder [24], a template-based Monte Carlo Tree Search (MCTS) algorithm trained on the USPTO reaction database. As detailed in Table 5, the generated molecules exhibited exceptional synthetic feasibility, with the algorithm identifying valid synthesis routes for 100.00% of the candidates within the specified search limits. This 100% solvability rate matches the ground-truth “Unique Good Scents” and “All Good Scents” datasets, indicating that the generative model implicitly learned chemically stable motifs amenable to standard organic transformations. Crucially, the “State Score”—a machine-learning-derived metric representing the confidence and feasibility of the identified routes (where 1.0 represents high confidence)—averaged 0.76 for the generated set. While slightly lower than the highly optimized commercial odorants in the Good Scents database (0.92–0.93), a score of 0.76 remains well within the range of experimentally actionable chemistry. The standard deviation of 0.27 in the generated set, compared to the tighter distributions of the training sets (0.15–0.17), reflects the model’s exploration of novel chemical space. The high solvability and low average step count (~ 2.89 steps) are likely influenced by the lower average molecular weight of the generated library, as smaller volatile molecules are generally more accessible from commercial precursors. This suggests the VAE is not merely memorizing easy-to-make training examples but is venturing into novel structural territories while retaining synthetic accessibility.

The practical viability of the generated candidates is further supported by route complexity metrics and precursor availability from the ZINC stock database. The generated molecules required, on average, 2.89 reaction steps to synthesize, a value that sits between the simple commercial odorants (1.61–1.85 steps) and the more complex general bioactive compounds in ChemBL (2.65 steps). This average step count of ~ 3 is ideal for industrial R&D, balancing structural novelty with process efficiency—a critical factor given that odorants are often low-molecular-weight (< 300 Da) compounds where long synthetic sequences are economically prohibitive. Furthermore, the analysis identified an average of 2.11 commercially available precursors in stock per generated molecule, surpassing the availability metrics for both the unique Good Scents (1.71) and ChemBL (1.71) datasets. This high precursor availability (average stock availability ratio of $> 70\%$ per route) significantly de-risks downstream experimental validation, as the majority of starting materials can be sourced directly rather than synthesized *de novo*. The finding that the generated set maintains short reaction pathways (max 25.00 routes found) using readily available building blocks confirms that the QSAR-guided latent space successfully encodes not just bioactivity and validity, but also the pragmatic constraints of synthetic organic chemistry.

Quantum chemical stability analysis

To validate the thermodynamic stability of the generated structures beyond simple geometric rules, we performed semi-empirical quantum mechanical calculations using the GFN2-xTB method [25]. This approach provides a rigorous assessment of the electronic ground state energy, offering a proxy for chemical stability. As shown in Figure 8b, the total energy distribution of the generated molecules aligns remarkably well with the ground-truth “Unique Good Scents” dataset. The generated molecules exhibited a mean total energy of -3.57 Hartree (Ha), compared to -2.85 Ha for the known odorants, with the slightly lower (more stable) energy in the generated set largely attributable to the minor molecular weight differences discussed previously. When normalized for molecular size, the energy per atom distributions are also statistically convergent. The generated molecules possess a mean energy per atom of -0.17 ± 0.12 Ha, which overlaps significantly with the Good Scents distribution (-0.11 ± 0.08 Ha). The low Kullback-Leibler divergence between the two distributions ($KL \approx 0.14$) confirms that the generative model does not produce high-energy, strained conformers or unstable electronic configurations. Instead, it successfully targets the thermodynamically favorable region of chemical space characteristic of stable, volatile organic compounds found in fragrance palettes.

a)



b)

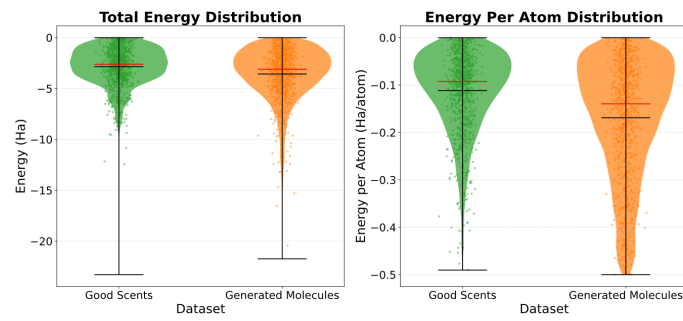


Figure 8. Synthesis accessibility and quantum chemistry checks. a) UMAP representation of seed and generated molecules encoded in the latent space color-coded by synthesis accessibility (SA – lower score relates to simpler synthesis complexity), b) comparison of total molecule and per atom energy calculations between generated molecules and Good Scents (ground truth molecules).

Comparative studies

Quantitative benchmarking against emerging generative frameworks reveals that the proposed QSAR-guided VAE offers a distinct balance of high novelty and industrial readiness. While Rodrigues et al. (2024) [26] utilize GNNs primarily for reformulation—explicitly excluding novel compounds to ensure database matches—and Sharma et al. (2025) [27] provide a valuable architectural benchmark of Diffusion and Transformer models, our framework is engineered specifically for *de novo* discovery. In terms of generative performance, our model matches the perfect validity of Sharma’s Diffusion model (100%) but significantly outperforms it in structural novelty (95.3% vs. 87.0%). Crucially, where Sharma’s Diffusion model exhibits high scaffold similarity (0.64), indicating a tendency toward derivatization, our VAE achieves a 74.4% rate of uncharted scaffold hops, discovering fundamentally new odorant cores. Additionally, our targeted QSAR model demonstrates superior discrimination (F1 score: 0.97) compared to the best-performing logistic benchmark in Sharma et al. (F1 score: 0.94). Finally, we address the “realism gap” identified as a limitation in these concurrent studies; by extending validation beyond heuristic rules to include 100% synthetic solvability (AiZynthFinder), ADMET safety profiling, and thermodynamic stability (GFN2-xTB), we provide the actionable downstream data required to transition generated candidates from theoretical algorithms to physical chemical development.

Rodrigues et al. (2024) employs Graph Neural Networks (GGNNs) for fragrance optimization but explicitly excludes novel chemical entities from the final selection, relying instead on “rediscovering” known catalogue compounds to ensure odor validity. In stark contrast, our framework does not merely retrieve knowns or generate theoretical structures; it actively discovers *de novo* entities, achieving a 74.4% rate of uncharted scaffold hops. Critically, we bridge the gap between generation and physical realization where other studies stop: while Rodrigues et al. validate via literature database lookups and Sharma et al. via computational rules, we provide a complete viability package comprising 100% synthetic solvability (AiZynthFinder), thermodynamic stability (GFN2-xTB), and safety profiling (ADMET), confirming the model’s utility for prospecting truly novel, manufacturable olfactory candidates.

Perspective and conclusions

We have presented an integrated VAE-QSAR framework that addresses the specific data scarcity challenges of olfactory science by combining property prediction with a self-learning generative architecture. By leveraging large-scale chemical data (ChemBL) to learn molecular syntax and refining the latent space with a specialized odor-prediction objective, the model successfully navigates beyond the boundaries of known odorants. The resulting architecture captures essential structural features while enabling the probabilistic exploration of novel chemical entities that remain physically realizable.

Benchmarking and Industrial Relevance: Quantitative benchmarking against emerging generative frameworks reveals that the proposed model occupies a distinct niche combining high generative novelty with rigorous industrial de-risking. While recent work by Rodrigues et al. (2024) [26] utilizes Graph Neural Networks primarily for reformulation—explicitly excluding novel compounds to ensure database matches—and Sharma et al. (2025) [27] provide a valuable architectural benchmark of Diffusion and Transformer models, our framework is engineered specifically for *de novo* discovery. In terms of generative performance, our model matches the perfect validity of Sharma’s Diffusion model (100%) but significantly outperforms it in structural novelty (95.3% vs. 87.0%). Crucially, where diffusion models often exhibit high scaffold similarity (0.64) indicating a tendency toward derivatization, our VAE achieves a 74.4% rate of uncharted scaffold hops. This confirms that the model is not merely optimizing side chains of known odorants but is actively discovering fundamentally new odorant cores.

Validation of the Discovery Pipeline: A critical limitation in generative molecular design is the “realism gap” between theoretical validity and experimental feasibility. We addressed this by extending validation beyond the heuristic “fragrance-likeness” rules often employed in the field. The model’s efficacy is supported by three pillars of evidence:

1. **Synthesizability:** Automated retrosynthetic analysis (AiZynthFinder) confirmed valid synthesis routes for 100% of candidates, with an average of 2.89 steps from commercially available precursors, demonstrating that generated novel scaffolds remain chemically accessible.
2. **Stability and Safety:** Quantum mechanical calculations (GFN2-xTB) verified that generated molecules occupy a thermodynamically stable region of chemical space, while ADMET profiling suggests a safety profile comparable to known commercial odorants.
3. **Generalization:** The model successfully generalized to the external ‘Unique Good Scents’ dataset (unseen during training). This confirms that the decision boundaries learned via SMOTE were biologically relevant rather than artifacts of oversampling, as evidenced by the alignment of the generated distribution with the ground truth manifold (FCD \approx 6.96).

Future Directions: While the current implementation focuses on the binary probability of odor, the structured latent space provides a foundation for fine-grained perceptual design. By conditioning the generative process on multi-label models (predicting specific descriptors like ‘woody’ or ‘citrus’), researchers could perform targeted inverse design, identifying regions of the latent space associated with complex organoleptic profiles. Furthermore, the confirmation of high synthetic accessibility ($> 70\%$ precursor availability) opens the door for accelerated closed-loop discovery cycles. Future work may integrate this generator with automated synthesis and high-throughput screening, using experimental feedback to iteratively refine the latent space mapping. This transition from purely computational generation to a de-risked, experimentally validatable pipeline represents a significant step toward systematically exploring the vast, unmapped regions of olfactory chemical space.

Acknowledgments

This research used the ALICE High Performance Computing facility at the University of Leicester. AI was in receipt of a Wellcome Trust Biomedical Vacation Scholarship.

Author contribution statement

Conceptualization: TCP, Methodology: AI, TCP. Programming: AI, TCP, Formal Analysis: AI, TCP, Investigation: AI, TCP. Writing – TCP. Visualization: AI, TCP.

References

1. C.S. Sell, Fundamentals of Fragrance Chemistry, Wiley-VCH, Weinheim, 2019.
2. L. Naldi, Assessment of the risk of fragrance allergy in the general population: challenges and methodological issues, *Drug Saf* 31 (2008) 440–443. <https://doi.org/10.2165/00002018-200831050-00012>.
3. F. Michailidou, The scent of change: sustainable fragrances through industrial biotechnology, *ChemBioChem* 24 (2023) e202300309. <https://doi.org/10.1002/cbic.202300309>.
4. K.A.D. Swift, P. Kraft, eds., Perspectives in flavor and fragrance research, Royal Society of Chemistry (Great Britain), Society of Chemical Industry (Great Britain), Verlag Helvetica Chimica Acta, Zurich, 2005. <https://doi.org/10.1002/9783906390475>.

5. K. Touhara, L.B. Vosshall, Sensing odorants and pheromones with chemosensory receptors, *Annual Review of Physiology* 71 (2009) 307-332. <https://doi.org/10.1146/annurev.physiol.010908.163209>.
6. S.M. Kurian, R.G. Naressi, D. Manoel, A.-S. Barwick, B. Malnic, L.R. Saraiva, Odor coding in the mammalian olfactory epithelium, *Cell Tissue Res* 383 (2021) 445-456. <https://doi.org/10.1007/s00441-020-03327-1>.
7. C. Bushdid, M.O. Magnasco, L.B. Vosshall, A. Keller, Humans can discriminate more than 1 trillion olfactory stimuli, *Science* 343 (2014) 1370-1372. <https://doi.org/10.1126/science.1249168>.
8. A. Zhavoronkov, Y.A. Ivanenkov, A. Aliper, M.S. Veselov, V.A. Aladinskiy, A.V. Aladinskaya, V.A. Terentiev, D.A. Polykovskiy, M.D. Kuznetsov, A. Asadulaev, Y. Volkov, A. Zholus, R.R. Shayakhmetov, A. Zhebrak, L.I. Minaeva, B.A. Zagribelnyy, L.H. Lee, R. Soll, D. Madge, L. Xing, T. Guo, A. Aspuru-Guzik, Deep learning enables rapid identification of potent DDR1 kinase inhibitors, *Nat Biotechnol* 37 (2019) 1038–1040. <https://doi.org/10.1038/s41587-019-0224-x>.
9. C.W. Coley, Defining and exploring chemical spaces, *Trends in Chemistry* 3 (2021) 133–145. <https://doi.org/10.1016/j.trechm.2020.11.004>.
10. J. Meyers, B. Fabian, N. Brown, De novo molecular design and generative models, *Drug Discovery Today* 26 (2021) 2707–2715. <https://doi.org/10.1016/j.drudis.2021.05.019>.
11. B. Sanchez-Lengeling, A. Aspuru-Guzik, Inverse molecular design using machine learning: Generative models for matter engineering, *Science* 361 (2018) 360–365. <https://doi.org/10.1126/science.aat2663>.
12. T. Yoshizawa, S. Ishida, T. Sato, M. Ohta, T. Honma, K. Terayama, A data-driven generative strategy to avoid reward hacking in multi-objective molecular design, *Nat Commun* 16 (2025) 2409. <https://doi.org/10.1038/s41467-025-57582-3>.
13. S. Liu, D. Zhang, Z. Tu, H. Dai, P. Liu, Evaluating molecule synthesizability via retrosynthetic planning and reaction prediction, (2025). <https://doi.org/10.48550/arXiv.2411.08306>.
14. E.J. Mayhew, C.J. Arayata, R.C. Gerkin, B.K. Lee, J.M. Magill, L.L. Snyder, K.A. Little, C.W. Yu, J.D. Mainland, Transport features predict if a molecule is odorous, *Proceedings of the National Academy of Sciences* 119 (2022) e2116576119. <https://doi.org/10.1073/pnas.2116576119>.
15. R. Gómez-Bombarelli, J.N. Wei, D. Duvenaud, J.M. Hernández-Lobato, B. Sánchez- Lengeling, D. Sheberla, J. Aguilera- Iparraguirre, T.D. Hirzel, R.P. Adams, A. Aspuru-Guzik, Automatic chemical design using a data-driven continuous representation of molecules, *ACS Cent. Sci.* 4 (2018) 268–276. <https://doi.org/10.1021/acscentsci.7b00572>.
16. H. Moriwaki, Y.-S. Tian, N. Kawashita, T. Takagi, Mordred: a molecular descriptor calculator, *Journal of Cheminformatics* 10 (2018) 4. <https://doi.org/10.1186/s13321-018-0258-y>.
17. N.V. Chawla, K.W. Bowyer, L.O. Hall, W.P. Kegelmeyer, SMOTE: synthetic minority over-sampling technique, *Journal of Artificial Intelligence Research* 16 (2002) 321–357. <https://doi.org/10.1613/jair.953>.
18. D.W. Hosmer, S. Lemeshow, R.X. Sturdivant, *Applied Logistic Regression*, 3. Aufl, Wiley, Hoboken, N.J, 2013.
19. Mordred 1.2.1a1 documentation, (n.d.). <https://mordred-descriptor.github.io/documentation/master/> (accessed April 22, 2025).
20. D. Mendez, A. Gaulton, A.P. Bento, J. Chambers, M. De Veij, E. Félix, M.P. Magariños, J.F. Mosquera, P. Mutowo, M. Nowotka, M. Gordillo-Marañón, F. Hunter, L. Junco, G. Mugumbate, M. Rodriguez-Lopez, F. Atkinson, N. Bosc, C.J. Radoux, A. Segura-Cabrera, A. Hersey, A.R. Leach, ChEMBL: towards direct deposition of bioassay data, *Nucleic Acids Research* 47 (2019) D930–D940. <https://doi.org/10.1093/nar/gky1075>.
21. K. Preuer, P. Renz, T. Unterthiner, S. Hochreiter, G. Klambauer, Fréchet ChemNet Distance: A Metric for Generative Models for Molecules in Drug Discovery, *Journal of Chemical Information and Modeling* 58 (2018) 1736–1741 <https://doi.org/10.1021/acs.jcim.8b00234>
22. M. Bezaatpour, M. Dal Maso, M. Rissanen, VaPORs v1.0.1: an automated model for functional group detection and property prediction of organic compounds via SMILES notation, *Geosci. Model Dev.*, 18 (2025) 9189–9217, <https://doi.org/10.5194/gmd-18-9189-2025>
23. K. Swanson, et al., ADMET-AI: a machine learning ADMET platform for evaluation of large-scale chemical libraries, *Bioinformatics*, 40(12) (2024) btae416. <https://doi.org/10.1093/bioinformatics/btae416>
24. S. Genheden, A. Thakkar, V. Chadimová, J-L. Bernstein, O. Engkvist, E. J. Bjerrum, AiZynthFinder: a fast, robust and flexible open-source software for retrosynthetic planning, *Journal of Cheminformatics* 12(1) (2020) 35. <https://doi.org/10.26434/chemrxiv.12465371.v1>

25. C. Bannwarth, S. Ehlert, S. Grimme, GFN2-xTB—An accurate and broadly parametrized self-consistent tight-binding quantum chemical method with multipole electrostatics and density-dependent dispersion contributions, *Journal of Chemical Theory and Computation* 15(3) (2019) 1652–1671. <https://doi.org/10.1021/acs.jctc.8b01176>
26. B.C.L. Rodrigues, V.V. Santana, S. Murins, I.B.R. Nogueira, Molecule Generation and Optimization for Efficient Fragrance Creation, *Ind. Eng. Chem. Res.* 63 (2024) 14667–14681. <https://doi.org/10.1021/acs.iecr.4c00650>
27. M. Sharma, S. Balaji, P. Saha, R. Kumar, Navigating the Fragrance Space Using Graph Generative Models and Predicting Odors. *Journal of Chemical Information and Modeling* 65(10) (2025) 4818–4832. <http://doi.org/10.1021/acs.jcim.5c00209>